Massive perturbations to atmospheric sulfur in the aftermath of the Chicxulub impact

Christopher K. Junium[a,1,2] ⓘ, Aubrey L. Zerkle[b,1,2] ⓘ, James D. Witts[c] ⓘ, Linda C. Ivany[a] ⓘ, Thomas E. Yancey[d] ⓘ, Chengjie Liu[e] ⓘ, and Mark W. Claire[b] ⓘ

Sulfate aerosols have long been implicated as a primary forcing agent of climate change and mass extinction in the aftermath of the end-Cretaceous Chicxulub bolide impact. However, uncertainty remains regarding the quantity, residence time, and degree to which impact-derived sulfur transited the stratosphere, where its climatic impact would have been maximized. Here, we present evidence of mass-independent fractionation of sulfur isotopes (S-MIF) preserved in Chicxulub impact ejecta materials deposited in a marine environment in the Gulf Coastal Plain of North America. The mass anomalous sulfur is present in Cretaceous–Paleogene event deposits but also extends into Early Paleogene sediments. These measurements cannot be explained by mass conservation effects or thermochemical sulfate reduction and therefore require sulfur-bearing gases in an atmosphere substantially different from the modern. Our data cannot discriminate between potential source reaction(s) that produced the S-MIF, but stratospheric photolysis of SO_2 derived from the target rock or carbonyl sulfide produced by biomass burning are the most parsimonious explanations. Given that the ultimate fate of both of these gases is oxidation to sulfate aerosols, our data provide direct evidence for a long hypothesized primary role for sulfate aerosols in the postimpact winter and global mass extinction.

K-Pg extinction | sulfur isotopes | mass-independent fractionation | mass extinction | sulfur cycle

The Chicxulub impact 66 Mya rearranged the balance of Earth's biosphere. From a human perspective, this was arguably the most important moment in Earth's history, as not only did an estimated 76% of all marine animal species and 40% of genera go extinct (1, 2) but mammals capitalized on an ecological vacuum and diversified to dominance in its wake (3, 4). Asteroid impacts are a relatively common occurrence in Earth history, yet in the instance of the Cretaceous–Paleogene (K-Pg) boundary, unequivocal evidence links a bolide impact to one of the largest mass extinctions of the Phanerozoic (5). What sets the Chicxulub event apart?

The Chicxulub impact vaporized evaporite and organic matter–bearing marine carbonates, injecting sulfur-bearing gases into the atmosphere in addition to CO_2, soot, and dust (6–9), potentially magnifying its effects. Atmospheric sulfur rapidly forms sulfate aerosols, which, if lofted into the stratosphere, scatter incoming solar radiation and can prolong planetary-scale cooling for many years after the impact-generated plume has dissipated (10, 11). Thus, sulfate aerosol–induced global cooling, sulfuric acid rain, and reduction of surface light for photosynthesis have been proposed as primary kill mechanisms following the K-Pg impact (5, 7, 8, 12, 13). Estimates of sulfur ejected during the K-Pg event range from 30 to 540 Gt, and climate models that account for this sulfur suggest 2 to 8 °C global cooling of Earth's surface for up to 13 y (10). Recent data from the Chicxulub peak ring suggest that these sulfur loads may have been vastly underestimated (6), raising the potential for even more severe consequences. Their impact on climate, however, depends on the height of injection into the atmosphere. Long-term cooling only occurs if generated aerosols form in the stratosphere, where they have residence times of years to decades. By contrast, tropospheric aerosols are efficiently removed in a matter of weeks. Additional constraints on sulfur mass, plume chemistry, and height of injection are thus needed to better estimate the effects of the Chicxulub impact on climate.

Mass-independent fractionation of sulfur isotopes (S-MIF) occurs during a number of gas-phase reactions (14–16). The S-MIF record has revolutionized the quantification of oxygen in Earth's atmosphere during the Archean and Early Paleoproterozoic, where S-MIF signatures are well-preserved in the rock record prior to the Great Oxidation Event (GOE), 2.43 billion years ago (17, 18). By contrast, S-MIF produced in oxic atmospheres is erased by the subsequent redox cycling of sulfur and the large reservoir size of sulfate at Earth's surface, where mass-dependent fractionation (MDF)

Author affiliations: [a]Department of Earth and Environmental Sciences, Syracuse University, Syracuse, NY 13244; [b]School of Earth and Environmental Sciences, Centre for Exoplanet Science, University of St Andrews, St Andrews KY16 9AL, United Kingdom; [c]School of Earth Sciences, University of Bristol, Bristol BS8 1RJ, United Kingdom; [d]The College of Geosciences, Texas A&M University, College Station, TX 77483; and [e]Ellington Geological Services, Houston, TX 77043

predominates, and hence S-MIF preservation in the post-Paleoproterozoic rock record, has never been demonstrated. While ephemeral on geologic timescales, records from polar ice cores (19–21) and snow pits (22, 23) do record time-dependent S-MIF signatures in sulfate aerosol particles. Given tropospheric sulfate aerosol residence times of days to weeks, the polar S-MIF records are interpreted to require stratospheric sulfate aerosols, which have lifetimes of years, thus enabling global transport and effects on climate.

Here, we present measurements of S-MIF anomalies that are recorded in K-Pg impact debris and overlying sediments, indicating wide-scale S-MIF in sulfur gases during the boundary event and their subsequent preservation in the sedimentary record. The preservation of this signal in a marine shelf environment requires that massive amounts of sulfur were injected into the stratosphere in the aftermath of the Chicxulub impact, providing direct, empirical evidence for the role of S-bearing gases in driving a postimpact winter and contributing to the mass extinction event. Further study of terrestrial and proximal marine K-Pg sequences combined with numerical modeling will help quantify the total sulfur load and associated, climatically active sulfate aerosols.

Geologic Setting

The S-MIF signal is archived in rocks of the US Gulf Coastal Plain, ~1,300 km from the impact site. Upper Cretaceous and lower Paleogene sediments exposed along the Brazos River and its tributaries in Falls County, Texas, comprise an exceptionally well-preserved and continuous succession across the K–Pg boundary (24–27), reflecting open marine deposition ~100 km from shore (28) and close to the mouth of the remnant Western Interior Seaway. Marine muds of the Cretaceous Corsicana Formation are capped by clastic deposits interpreted to be the result of postimpact seismicity, tsunami activity, storms, and atmospheric fallout and contain abundant carbonate lapilli and ejecta spherules (28, 29). The overlying Paleogene Kincaid Formation represents a return to normal marine sedimentation. The sampled sections along Darting Minnow Creek (DMC) encompass the uppermost Maastrichtian Corsicana Formation, the K-Pg event deposit, and the Littig Member of the Kincaid Formation. Sampled intervals of the Littig Member contain microfossils diagnostic of Danian planktonic foraminiferal Zone P0 and calcareous nannofossil Zone NP1, deposited during the initial 40,000 y following the impact, extending into the Pα Zone (Fig. 1 and *SI Appendix*) (30).

Results

The abundance of sulfur in the impact sequences ranges from 0.4 to 5.1 weight percent (wt. %) and is highly variable compared to background mudstones, which range from 0.7 to 1.4 wt. %. The molar organic carbon to total sulfur ratios ($C_{org}:S_{tot}$) within the impact debris average 0.9 and are significantly lower than the bounding mudstones which average 3.8 (*SI Appendix*, Tables S1 and S2). Chromium-reducible sulfur phases from the DMC rocks have $\Delta^{33}S$ signatures that are as low as −0.32‰ in the postimpact depositional sequence and persist into lowermost Paleogene (P0 Zone) mudstones that immediately overlie impact-related event deposits. These $\Delta^{33}S$ values are significantly offset from the Maastrichtian and Danian marine sulfides that range from +0.02 to +0.08‰, with a mean $\Delta^{33}S$ value of +0.04‰. The $\Delta^{36}S$ values range from +2.12 to −0.67‰ (Figs. 1 and 2 and *SI Appendix*, Tables S1
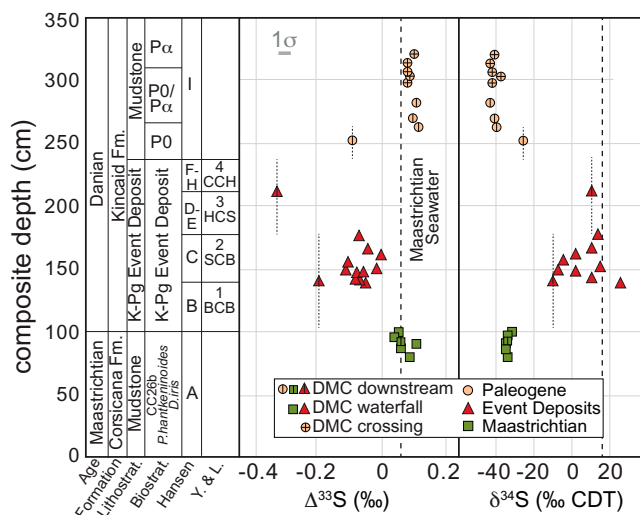

Fig. 1. Sulfur isotope data ($\delta^{34}S$ and $\Delta^{33}S$) from chromium-reducible sulfur. The study interval reported here is relative to a composite depth scale, reflecting the stratigraphy of three sections exposed along DMC, which are separated by ~200 m. Biostratigraphic and lithologic designations are modified from Yancey and Liu (28) and Hansen (24) (see *SI Appendix* for details on stratigraphic correlations and new biostratigraphic data). The small, vertical dashed lines reflect the composite depth interval of samples taken from the condensed DMC "downstream" section. Basal Conglomerate Bed (BCB), Spherulitic Conglomerate Bed (SCB), Hummocky-Sandstone Unit (HSU) and Calcareous Clayey Horizon (CCH) are K-Pg event deposit units defined by Yancey and Liu (28).

and S2). The underlying Maastrichtian Corsicana Formation and overlying Danian Kincaid Formation mudstones above P0 Zone have $\Delta^{33}S$ and $\Delta^{36}S$ values that are similar to marine sulfates from the End Cretaceous (31). The $\delta^{34}S$ values of these sulfides range from −41.4 to +23.6‰. The ^{34}S-enrichment contained within the ejecta materials (mean of +7.6‰) is offset from the encasing strata and suggest that the sulfur was derived from the target rock evaporites (32). Previous efforts to evaluate the presence of impactor-derived elemental sulfur with expected $\delta^{34}S$, $\delta^{33}S$, and $\delta^{36}S$ values near 0‰ were unsuccessful in identifying an extraterrestrial sulfur source in the Brazos River impact deposits (33). Rather, the results of a single sample for multiple sulfur isotope analyses were interpreted to be consistent with a terrestrial, microbially mediated sulfur cycle signal with $\delta^{33}S$, $\delta^{34}S$, and $\delta^{36}S$ values that were −12.97, −24.89, and −46.4‰, respectively. On their own, the small $\Delta^{33}S$ (−0.07‰) and $\Delta^{36}S$ (+0.12‰) anomalies measured in that study were not considered diagnostic of an S-MIF origin. However, when taken in the context of our larger dataset, the results of Heymann et al. (33) are entirely consistent with our results from within the ejecta materials (Fig. 1).

Discussion

Small but measurable $\Delta^{33}S$ values (generally 0 ± 0.10‰) are relatively common in modern sedimentary and aqueous settings and in rocks of Late Proterozoic and Phanerozoic Age. The majority of small-magnitude $\Delta^{33}S$ anomalies are rooted in biogeochemical sulfur cycling and are not the result of atmospheric processes causing mass-independent fractionation. If atmospheric S-MIF is to be confirmed, the range of mass-dependent processes capable of producing anomalies in $\Delta^{33}S$ (and $\Delta^{36}S$, although these are much less well constrained) must first be ruled out.

MDF during microbial sulfur cycling can cause small deviations in $\Delta^{33}S$ (34–36). Equilibrium fractionations result in an
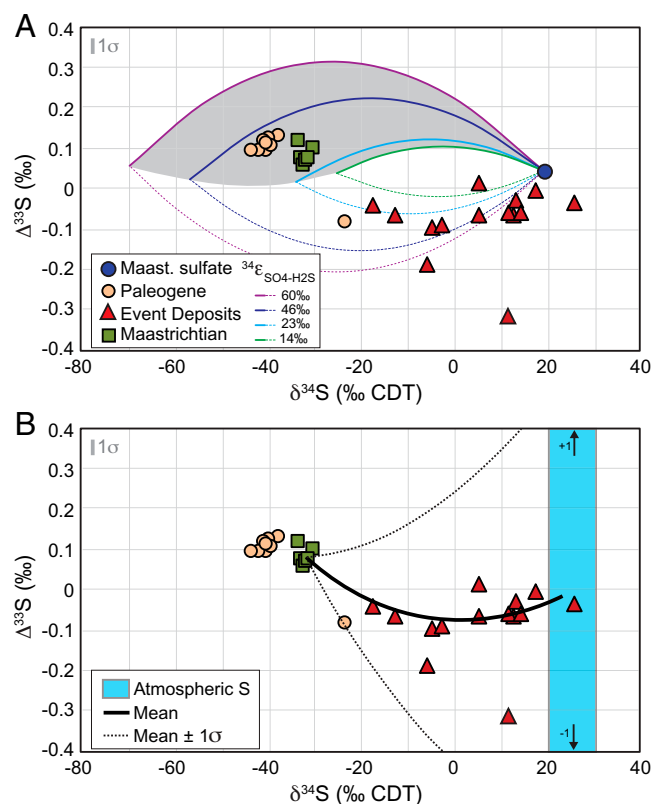
Fig. 2. Cross-plots of $\delta^{34}S$ and $\Delta^{33}S$ data. The upper shaded region in A shows the results of a sulfur cycle box model [modified from (34)] that produces minor deviations in $\Delta^{33}S$ resulting from mass conservation effects (MCE). MCE occur during microbial sulfur cycling, here modeled at four specific fractionation factors (colored lines) for microbial sulfate reduction, using the $\delta^{34}S$ and $\Delta^{33}S$ of Maastrichtian seawater sulfate as an initial condition (31). Colored dashed lines further indicate the results of a mixing model between Maastrichtian seawater sulfate isotope values and these generated sulfides, showing how mixing processes could produce negative deviations in $\Delta^{33}S$, albeit smaller than those we measure here. B shows the results of a second mixing model that combines one sulfur end member with an S-MIF signature approximating volcanically derived sulfates with a second sulfur end member with a sulfur MDF signature similar to preevent pyrite. This model, which most closely reproduces our data, shows the mean ± 1σ of sulfur products produced by varying the S-MIF end member from +1 to −1‰ in $\Delta^{33}S$ using a Monte Carlo method.

exponential relationship between $\delta^{33}S$ and $\delta^{34}S$, whereas mixing between sulfur pools within metabolic networks are linear, causing small deviations in $\Delta^{33}S$ from the predicted reference array . At the ecosystem level, these mass conservation effects (MCE) are the product of multistep sulfur cycling via processes such as sulfate reduction, sulfur oxidation, and sulfur compound disproportionation acting on seawater sulfate. MCE can produce deviations in $\Delta^{33}S$ and $\Delta^{36}S$ that are recognizable by their small magnitude and by characteristic ^{33}S-^{34}S-^{36}S systematics (34–37). To explore the possibility of MCE in the context of our data, we employed a sulfur cycle box model that includes sulfate reduction, sulfide/sulfur oxidation, and sulfur disproportionation to investigate potential MCE (Fig. 2A). The results of the model yield a range of $\delta^{34}S$ and $\Delta^{33}S$ values for resulting sulfides that encompass the Maastrichtian and the majority of the Paleogene samples, consistent with MDF of sulfur isotopes via an active marine sulfur cycle. However, this model cannot reproduce the negative $\Delta^{33}S$ values from the impact deposits or the lowermost Paleogene (Fig. 2A), requiring additional sulfur-cycling processes.

Previous work has also demonstrated that small, negative $\Delta^{33}S$ values ($\sim -0.1‰$) can be produced during mixing between pyrite produced by near-quantitative reduction of marine sulfate (small apparent fractionation and sulfur isotope compositions equivalent to marine sulfate) and pyrite produced by a similar marine sulfur cycle (large apparent fractionation and sulfur isotope compositions offset from sulfate). This process has been proposed to explain small, negative $\Delta^{33}S$ values in End Permian sediments and interpreted to represent an incursion of sulfidic waters associated with the P-Tr extinction event (38). We explored this possibility for the K-Pg by using a mixing model, in which sulfur with an isotopic composition of Late Maastrichtian seawater (31) is mixed with pyrite of a range of isotopic compositions derived from our marine sulfur–cycling model (encompassed by the lower dashed lines in Fig. 2A). If similar mixing processes were the primary explanation for our data, we would expect this mixing model to encompass all of our $\Delta^{33}S/\delta^{34}S$ data (Fig. 2A). However, these mixing models can only reproduce some of our data and largely require mixing with extreme end members of biologically produced pyrite from the ocean model to do so, which might not be realistic. Overall, these mixing models cannot reproduce the majority of the $\Delta^{33}S$ values associated with impact deposits, again requiring other sulfur-cycling processes.

Left without a realistic scenario whereby the impact deposit sulfur isotope values can be produced via mass-dependent, sulfur-cycling processes alone, we next explore processes known to produce S-MIF. Thermochemical sulfate reduction (TSR) is the only nonatmospheric process that has been shown to induce large S-MIF. TSR is caused by a magnetic isotope effect, which only affects odd number isotopes, producing positive $\Delta^{33}S$ values up to +13‰ without a corresponding $\Delta^{36}S$ anomaly (39). The rocks of the Corsicana and Kincaid formations are thermally immature and display no veining or other geologic evidence of postdepositional, hydrothermal alteration that might induce TSR. Critically, the DMC section shows $\Delta^{36}S$ values that are negatively correlated to $\Delta^{33}S$ (Fig. 3), inconsistent with magnetic isotope effects formed during TSR.

By exclusion of a suitable, biological, mixing, or thermochemical mechanism, the negative $\Delta^{33}S$ values of the Brazos River impact event deposits and lowermost Paleogene samples must have been produced by gas-phase reactions between S-bearing gases, a number of which have been demonstrated to create mass-independent sulfur isotope anomalies (16, 23). Stratospheric injection of sulfur gases during Plinian-style volcanic eruptions produce $\Delta^{33}S$ anomalies that range from +2 to −2‰ in sulfate aerosols that are preserved in ice cores (19–21). The ice core records display an evolution in $\Delta^{33}S$ values that are consistent with spatial and temporal separation during oxidation of SO_2 to sulfate that maintains an isotopic mass balance in $\Delta^{33}S$, following the evolution of eruption-derived sulfates across multiple years (21). While photochemical models remain unable to fully predict multiple sulfur isotopes using known fractionation factors (40), production of S-MIF has been experimentally demonstrated to arise from SO_2 photolysis and self-shielding under modern stratospheric conditions (15), providing a reasonable, potential analog for the postimpact atmosphere.

A candidate source for S-MIF could be sulfur liberated during extensive biomass burning (6, 8, 15). Biomass burning imparts small-magnitude S-MIF on resulting combustion products, with $\Delta^{33}S$ values as low as −0.19‰ observed in combustion experiments (41). Though a potential contributor, a direct, biomass-burning signal alone would only have been capable of achieving the $\Delta^{33}S$ values we observe in the Brazos sediments if biomass-derived sulfur was the dominant sedimentary source,
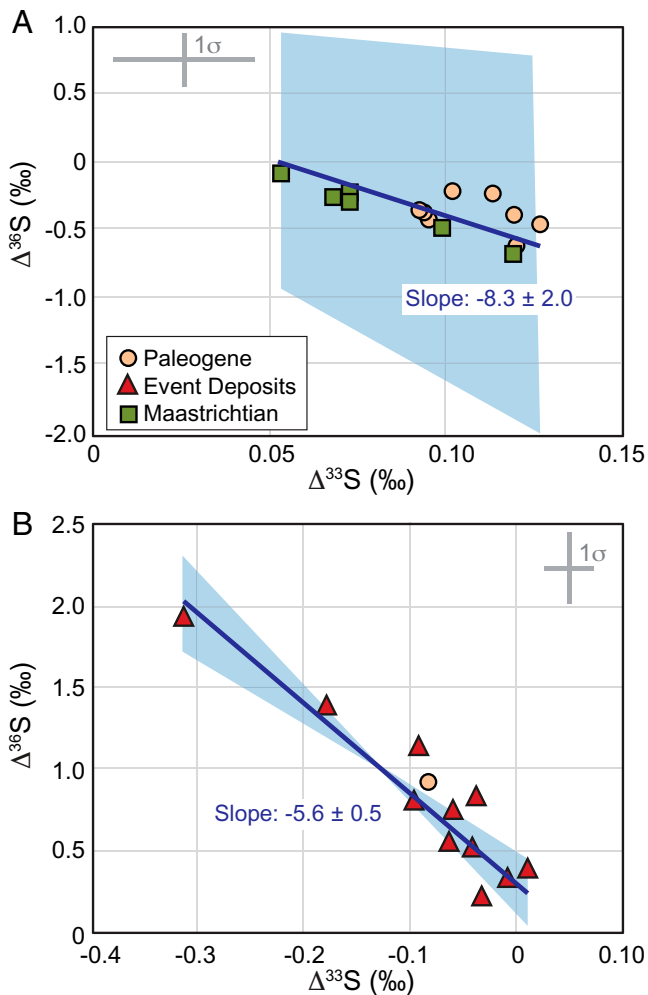
Fig. 3. Orthogonal data regression (17) showing $\Delta^{36}S/\Delta^{33}S$ slopes and 3σ CIs of the regression (shaded region) for Maastrichtian and Paleogene samples (*A*) and for samples with ejecta materials within the impact event bed deposits and the sample from the basal Paleogene that overlies the event bed deposits (*B*).

which is unlikely. Rather, the fate of the sulfur aerosols that are formed during biomass burning provide a more likely candidate for carrying an S-MIF signature that is geologically relevant. For example, the sulfur isotope record in South Pole snow pits have $\Delta^{33}S$ anomalies up to +1.6‰, much larger than those observed for Plinian-style eruptions and are the result of massive, biomass-burning events (22). The biomass-burning $\Delta^{33}S$ anomalies are carried in stratospheric sulfate aerosols that are the transformation products of OCS produced during biomass burning (42, 43). OCS is a tropospherically inert gas that can transit the tropopause where OCS is oxidized to SO_2 in the stratosphere, ultimately resulting in the formation of high-altitude sulfate aerosols (42) that carry MIF signatures and are distributed globally (22).

Another potentially important source of sulfur following the impact was that in close association with fossil organic matter in the target rock (9), either as pyrite or organic sulfur. Organic matter–associated sulfur could have been pyrolyzed or burned and followed a reaction path similar to biomass burning, or it could have been incorporated into the ejecta plume and ultimately oxidized to SO_2 and photolyzed in the stratosphere. Therefore, while the presence of S-MIF in our samples cannot distinguish between these possible atmospheric sulfur sources, our data provide direct, empirical evidence that sulfate aerosols

were in the stratosphere, as previously only suggested by impact theory (7, 44).

Unlike the subannually resolved records in ice cores (19–21), the DMC rocks only record a negative anomaly in $\Delta^{33}S$, which raises questions regarding isotopic mass balance, given the lack of a compensatory, positive $\Delta^{33}S$ shift. In order to quantitatively address this, we employed an additional Monte Carlo isotope-mixing model to examine the cumulative, sedimentary signature of mixing preevent sulfur with an atmospherically produced $\Delta^{33}S$ signal similar to that observed in ice cores (Fig. 2*B*). Notably, this model requires atmospheric end members with $\Delta^{33}S$ values varied between +1 to −1‰ to capture the entirety of the K-Pg impact deposit data. The +1 to −1‰ range of $\Delta^{33}S$ values in our model is consistent with those observed during Plinian-style volcanic eruptions and periods of enhanced biomass burning, so both mechanisms remain plausible for the production of S-MIF signatures in the aftermath of the Chicxulub impact. However, we should note that even high-resolution studies of modern, volcanically produced S-MIF do not always resolve an isotopic mass balance, and despite the relative completeness of the Brazos River sedimentary record, it is possible that this only partially preserves the S-MIF record due to temporal or spatial heterogeneities.

The slope between $\Delta^{36}S$ and $\Delta^{33}S$ values in our K-Pg sediments further supports an atmospherically produced S-MIF signal. Multiple sulfur isotope values in sediments deposited under oxic atmospheres generally have steep $\Delta^{36}S/\Delta^{33}S$ slopes (~-8) consistent with MCE from MDF processes, as observed in the post-GOE geologic record (36). A lower slope is typical of anoxic atmospheres (-0.9 ± 0.1) (15, 45), as observed in pre-GOE $\Delta^{36}S/\Delta^{33}S$ relationships and predicted by theory (16). The preimpact Maastrichtian and later Danian samples display a $\Delta^{36}S/\Delta^{33}S$ slope of -8.3 ± 2, consistent with MDF deposits (Fig. 3*B*). By contrast, the $\Delta^{36}S/\Delta^{33}S$ relationship in the K-Pg impact event samples from Brazos River has a shallower $\Delta^{36}S/\Delta^{33}S$ slope of -5.6 ± 0.5 (Fig. 3*B*), resting between the canonical Archean $\Delta^{36}S/\Delta^{33}S$ slope and the MDF slope. The relationship between $\Delta^{36}S$ and $\Delta^{33}S$ in our samples does not follow the typical Archean slope of -0.9 ± 0.1, but there is no reason to expect this relationship would be produced in an oxygenated Phanerozoic atmosphere. Instead, the $\Delta^{36}S/\Delta^{33}S$ slope in our data is consistent with those measured in recently deposited, volcanic sulfate aerosols from ice cores and volcanic ash layers (-2 to -6) (19, 46), suggesting a similar S-MIF formation pathway within the stratosphere, with or without mixing. It is possible that the unique slope in the impact-associated deposits compared to the surrounding strata is the result of a unique, stratospheric chemistry in the aftermath of the impact, but these values have almost certainly been modified by mixing with existing non-MIF–bearing marine sulfate.

In an oxidizing Cretaceous and Paleogene atmosphere (47), redox recycling of sulfur sourced from the atmosphere and the size of the marine sulfate reservoir (48) limit the likelihood that S-MIF signatures could be easily preserved. For example, even the largest volcanic eruptions of the last millennium increase the concentrations of sulfates in glacial ice by no more than 10 µM (21). Therefore, the preservation of S-MIF in marine sections requires a quantity and flux of atmospherically derived S-MIF to the basin sufficient to overwhelm the sulfur isotope composition of the local sulfate flux to the sediments (49) and any sulfur within the ejecta that was deposited too rapidly to accumulate an S-MIF signature (e.g., spherules and lapilli) or was not subject to the effects of impact-related conflagrations.

The location proximal to the impact, a relatively restricted circulation in an embayment at the mouth of the remnant Western Interior Seaway, and the large drainage area to water volume ratio within the embayment likely maximized the potential for preservation of these S-MIF anomalies. In addition, the persistence of an S-MIF signal into the lowermost Paleogene deposits requires that a repository of atmospherically derived sulfur remained on the continent, supplying an enhanced, MIF-bearing riverine sulfate input for upwards of 10 ka after the primary deposition to the drainage basin (50). We explore the feasibility of a persistent postimpact S-MIF flux scenario via a simple consideration of residence times. On the basis of estimates for the persistence of sulfate aerosols in the atmosphere, the flux of riverine sulfate, and the size of the marine sulfate reservoir, we estimate that S-MIF production and rainout could persist for 30 y with global coverage (*SI Appendix*).

While the atmosphere was certainly perturbed for a significant amount of time, S-MIF generation would occur on different timescales depending on the mechanism. If the S-MIF were generated during SO_2 photolysis with access to shortwave ultraviolet light, it is estimated that all of the sulfur would have been oxidized to sulfate within months (10). Biomass burning, by contrast, would provide S-MIF for as long as there was biomass to burn, but it is reasonable to expect that this interval of time would have been relatively short, on the order of days (15). Significant uncertainties remain, but it is clear that at least some of the S-MIF was generated in the earliest stages following the impact, given that S-MIF anomalies were included within the proximal and intermediate ejecta deposits that would have blanketed North America and elsewhere. The bulk of the MIF-bearing, soluble sulfate minerals would not have been preserved in place and would have weathered into the basin at variable rates over the subsequent years, providing nonsteady-state riverine fluxes of S-MIF–bearing sulfate into the Gulf Coastal Plain. We estimate that if 10% of the generated impact sulfur (4×10^{16} g) landed on North America and was available for weathering over 10^4 years, this would increase riverine sulfate flux to the basin by an order of magnitude, with residence times similar to that of ocean refresh, providing a unique opportunity for the preservation of an S-MIF signal into basal Paleogene deposits, as we observe (Fig. 1).

Despite these uncertainties, the Brazos River S-MIF data reveal constraints regarding the role of climatically reactive sulfur species in the postimpact environment. Sulfur has long been implicated in the environmental disturbance in the aftermath of the impact and as one of the primary causes of the extinction. However, these ideas have remained largely theoretical given lack of constraints on the timing of sulfate aerosol formation, the timescale of their removal, and the predominant sulfur species (7, 8). While our data do not preclude the presence of the more rapidly removed SO_3 (51), the S-MIF signatures provide the geochemical fingerprint that confirms the formation of stratospheric sulfate aerosols derived from impact-generated SO_2 and/or biomass burning. The presence of the S-MIF signatures throughout the K-Pg event deposit suggests that S-MIF production occurred during the earliest stages of the impact fallout and was not limited by lofting of sunlight-blocking dust and soot (7, 8). The persistence of the S-MIF signatures above the ejecta beds into the basal Danian sediments suggest that climatic effects of sulfate aerosols may have been longer than currently modeled estimates (8).

Given that the S-MIF anomalies in our samples are only found in rocks that contain ejecta materials and in the sediments immediately overlying the K-Pg sequence, we attribute this signal solely to the effects of the Chicxulub impact on the sulfur cycle, rather than to contemporaneous volcanism from the Deccan Traps Large Igneous Province, which are concentrated in the periods before and after the impact event (52, 53). It is thought that climatic effects of volcanically released CO_2 and SO_2 during Deccan eruptions were most apparent during the ~300 ka prior to the K-Pg boundary (54, 55). From the perspective of S-MIF, it is clear that the Maastrichtian record from Brazos River is characterized by a sulfur cycle that fits well within the Phanerozoic normal (Fig. 1). If sulfur gases were an important component of the early eruptive phase of the Deccan Traps prior to the impact, it is likely they were limited to tropospheric sulfur aerosols, which have relatively short residence times (weeks as opposed to years), limited distance of travel, and therefore limited ability to force cooling and affect the global sulfur cycle. By contrast, the lowest S-MIF values at Brazos River (Fig. 1) are within the interval in which there is evidence for significant cooling coincident with iridium (Ir) anomalies (56). The recognition of S-MIF in the Brazos River K-Pg event deposit confirms that sulfate aerosols were an integral component of the postimpact winter that was the proximate cause of the global mass extinction at the K-Pg boundary.

Materials and Methods

Sample Materials. Field-collected rock samples were removed from trenched and cleared outcrops and placed in labeled cotton or plastic bags. A suite of samples was collected from a small push core made at outcrop, subsequently sampled in the laboratory. Samples were dried and cleaned of exogenous debris. Materials selected for further analyses had any external surfaces removed by rock saw or knife to reveal unweathered surfaces and were subsequently powdered with a ball mill or mortar and pestle where appropriate.

Sulfide Extraction Methods. Sulfide extractions were performed in the Geobiology Laboratory at the University of St Andrews and in the Geobiology, Astrobiology, Paleoclimatology and Paleoceanography (GAPP) Laboratory at Syracuse University using the chromium reduction method (57). Because of high, extractable sulfur contents of the ejecta bed samples, we utilized 0.1 to 1.0 g powdered sample. Sample powders were loaded into condenser reaction vessels that are swept with nitrogen gas to remove atmospheric O_2. Samples were tested for the presence of acid-volatile sulfide with the addition of 20 mL 6-N hydrochloric acid and subsequently treated with 20 mL 1-M chromium chloride and refluxed for at least 2 h to ensure complete reaction of chromium-reducible sulfides. The resulting sulfide was trapped in a silver nitrate solution, and precipitates of silver sulfide were allowed to cure in the silver nitrate solution for at least 24 h, collected, rinsed with deionized water, dried, weighed, and stored in glass vials until analysis.

$\delta^{34}S$ Analysis Methods. The sulfur isotope compositions of silver sulfides were measured in the GAPP Laboratory at Syracuse University using an Elementar Isotope Cube elemental analyzer (EA) coupled to an Isoprime 100 isotope ratio mass spectrometer. Samples were loaded into tin capsules with vanadium pentoxide accelerant. EA conditions were as follows: helium purge was set for 45 s; oxidation and reduction reactor temperatures were 1,100 °C and 650 °C, respectively; helium carrier gas flow was 230 mL/min; the O_2 pulse was set for 75 s; and the SO_2 trap was heated to 230 °C. Samples were run comingled with International Atomic Energy Agency reference materials S1 (−0.30‰), S2 (+22.7‰), and S3 (−32.2‰). Generated SO_2 is analyzed as neoformed SO^+, resulting in better reproducibility compared to SO_2 analysis (58). Sample and standard data were corrected to accepted values for the reference materials using the correction scheme described in Coplen et al. (59). Reproducibility for replicate samples and standards was often better than ±0.20‰ but is reported here as ±0.20‰, reflecting the known isotope composition of the reference materials used in this study.

Sulfur and Organic Carbon Abundance Methods. Total sulfur and organic carbon contents were measured using EA conditions described in δ^{34}S Analysis Methods on crushed samples for total sulfur and on decarbonated samples for organic carbon content. Decarbonation was achieved using buffered acetic acid (pH 4). Calibration of the EA for S and C content was achieved using a sulfanilamide standard material (Elemental) (18.62 wt. % S and 41.84 wt. % C). Reproducibility of the S and C content is 0.5% relative SD for sulfanilamide in nitrogen-carbon-sulfur mode on the Elementar EA.

SF$_6$ Production and Analysis Methods. Sulfur isotope ratios (^{33}S/^{32}S, ^{34}S/^{32}S, and ^{36}S/^{32}S) are reported using the standard delta notation (δ) showing per mil (‰) deviations from international standard Vienna Cañon-Diablo Troilite (V-CDT), as follows:

$$\delta^{3X}S = \left[{}^{3X}S/{}^{32}S_{sample}/{}^{3X}S/{}^{32}S_{VCDT} - 1 \right] \times 1000,$$

where 3× is 33, 34, or 36. Minor S isotope values are further expressed using Δ^{33}S and Δ^{36}S notation, as the following:

$$\Delta^{33}S = \delta^{33}S - \left[\left({}^{34}S/{}^{32}S_{sample}/{}^{34}S/{}^{32}S_{VCDT} \right)^{0.515} - 1 \right]$$

$$\Delta^{36}S = \delta^{36}S - \left[\left({}^{34}S/{}^{32}S_{sample}/{}^{34}S/{}^{32}S_{VCDT} \right)^{1.90} - 1 \right].$$

Minor S isotope analyses (Δ^{33}S and Δ^{36}S) were conducted in the St Andrews Isotope Geochemistry laboratories at the University of St Andrews, using a modified Curie-point pyrolysis sulfur fluorination line, as described in Warke et al. (17). Briefly, 0.3 to 0.6 mg Ag$_2$S was weighed out into an iron–nickel–cobalt alloy pyrofoil with ≥50 times excess CoF$_3$ and placed in a borosilicate glass tube with ~1 g optical NaF crystals to consume HF. The reaction tube was placed in a JHP-22 Curie-point pyrolyser (Japan Analytical Industry), evacuated to vacuum, and flash heated to 590 °C for 297 s to produce SF$_6$ gas. The product gas was introduced into a bespoke vacuum line, in which it was purified through sequential cryogenic capture and gas chromatography. The final purified SF$_6$ was analyzed with a dedicated Finnigan MAT 253 dual-inlet mass spectrometer at m/z values of 127, 128, 129, and 131 (^{32}SF$_5^+$, ^{33}SF$_5^+$, ^{34}SF$_5^+$, and ^{36}SF$_5^+$), and assumed values for the reference SF$_6$ gas relative to the V-CDT scale are δ^{34}S = 5.86‰, Δ^{33}S = 0.013‰, and Δ^{36}S = −0.252‰ (18). The Δ^{33}S and Δ^{36}S values for IAEA-S1 produced by this method ($n = 80$) are 0.115 ± 0.015‰ and −0.581 ± 0.172‰ (mean ± 1σ), respectively, consistent with standard values published in the literature (60, 61). The precision of a single measurement was typically in the range of 0.01‰ for Δ^{33}S and 0.1‰ for Δ^{36}S.

Description of Atmospheric Sulfate Mass Balance Estimates. We estimate between 1 to 6 × 10^{16} g sulfate in the basin using estimates of paleobasin size [0.14% of Earth surface area and 85-m water depth (28, 62)] and

Maastrichtian seawater sulfate concentrations which range from 2 to 10 mM (48, 63–66). The current Gulf of Mexico catchment area is ~1% of Earth's surface area, assuming 1% of the total modern riverine sulfate (55) predicts a background riverine sulfate flux to the basin of 4 × 10^{11} g/S/y, for a first-order sulfate residence time against terrestrial rivers of ~10^5 y. By contrast, the estimated rate of inflow to the Brazos River region of the Gulf Coastal Plain [3 × 10^{13} m^3/y to Western Interior seaway (67)] provides a sulfate residence time against marine refresh of 10^3 to 10^4 y, which therefore would have controlled the preimpact basinal sulfate concentration. Total sulfur volatilization was conservatively estimated at 4 × 10^{17} g/S, but this would not have been uniformly distributed over the globe, given the clear difference in the thickness of K-Pg boundary deposits with proximity to the Chicxulub crater (1). Proximal (<1,500 km) sites in the Gulf of Mexico (such as Brazos River) contain decimeter thick, coarse-grained event deposits, with ejecta spherules, shocked minerals, and lapilli along with sedimentological features indicative of rapid deposition, overlain by multiple minor Ir anomalies representing later atmospheric fallout of particulate material. Intermediate sites in the Western Interior of the United States and Canada show 1- to 10-cm thick boundary deposits, while distal (Europe, Africa, Asia, and Pacific Ocean) sites contain only 2- to 5-mm thick event deposits, with ejecta virtually coincident with a single Ir anomaly. While sedimentation rates and timing remain debated at many sites, it is clear that far more ejecta material was deposited closer to the impact than farther afield, and it likely contained abundant sulfur derived from the Chicxulub impact, similar to the Brazos River sediments. While explicit timescales are not resolvable from the current stratigraphy, our most basal Paleogene sulfur isotope data suggest continental weathering of sulfur MIF-bearing material deposited in the ~30-y postimpact continued to influence the basin into the earliest Paleogene. While uncertainties in these calculations are undoubtedly large, conservative mass balance estimates are consistent with riverine sulfur input, influencing the basin for 10^4 y following the impact.

Data Availability. All study data have been uploaded to the Dryad open access database (https://doi.org/10.5061/dryad.0zpc8670h) and are also included in the article and/or *SI Appendix*.

1. D. Jablonski, Extinctions in the fossil record. *Philos. Trans. R. Soc. Lond. B Biol. Sci.* **344**, 11–17 (1994).
2. R. K. Bambach, A. H. Knoll, S. C. Wang, Origination, extinction, and mass depletions of marine diversity. *Paleobiology* **30**, 522–542 (2004).
3. J. Alroy, The fossil record of North American mammals: Evidence for a Paleocene evolutionary radiation. *Syst. Biol.* **48**, 107–118 (1999).
4. T. J. D. Halliday, P. Upchurch, A. Goswami, Eutherians experienced elevated evolutionary rates in the immediate aftermath of the Cretaceous-Palaeogene mass extinction. *Proc. Biol. Sci.* **283**, 20153026 (2016).
5. P. Schulte *et al.*, The Chicxulub asteroid impact and mass extinction at the Cretaceous-Paleogene boundary. *Science* **327**, 1214–1218 (2010).
6. S. P. S. Gulick *et al.*; Expedition 364 Scientists, The first day of the Cenozoic. *Proc. Natl. Acad. Sci. U.S.A.* **116**, 19342–19351 (2019).
7. O. B. Toon, C. Bardeen, R. Garcia, Designing global climate and atmospheric chemistry simulations for 1 and 10 km diameter asteroid impacts using the properties of ejecta from the K-Pg impact. *Atmos. Chem. Phys.* **16**, 13185–13212 (2016).
8. C. R. Tabor, C. G. Bardeen, B. L. Otto-Bliesner, R. R. Garcia, O. B. Toon, Causes and climatic consequences of the impact winter at the Cretaceous-Paleogene boundary. *Geophys. Res. Lett.* **47**, e60121 (2020).
9. S. L. Lyons *et al.*, Organic matter from the Chicxulub crater exacerbated the K-Pg impact winter. *Proc. Natl. Acad. Sci. U.S.A.* **117**, 25327–25334 (2020).
10. E. Pierazzo, A. N. Hahmann, L. C. Sloan, Chicxulub and climate: Radiative perturbations of impact-produced S-bearing gases. *Astrobiology* **3**, 99–118 (2003).
11. K. O. Pope, K. H. Baines, A. C. Ocampo, B. A. Ivanov, Impact winter and the Cretaceous/Tertiary extinctions: Results of a Chicxulub asteroid impact model. *Earth Planet. Sci. Lett.* **128**, 719–725 (1994).
12. M. J. Henehan *et al.*, Rapid ocean acidification and protracted Earth system recovery followed the end-Cretaceous Chicxulub impact. *Proc. Natl. Acad. Sci. U.S.A.* **116**, 22500–22504 (2019).
13. J. Brugger, G. Feulner, S. Petri, Baby, it's cold outside: Climate model simulations of the effects of the asteroid impact at the end of the Cretaceous. *Geophys. Res. Lett.* **44**, 419–427 (2017).
14. Y. Lin, M. S. Sim, S. Ono, Multiple-sulfur isotope effects during photolysis of carbonyl sulfide. *Atmos. Chem. Phys.* **11**, 10283–10292 (2011).
15. Y. Endo, S. O. Danielache, Y. Ueno, Total pressure dependence of sulfur mass-independent fractionation by SO$_2$ photolysis. *Geophys. Res. Lett.* **46**, 483–491 (2019).
16. D. Babikov, Recombination reactions as a possible mechanism of mass-independent fractionation of sulfur isotopes in the Archean atmosphere of Earth. *Proc. Natl. Acad. Sci. U.S.A.* **114**, 3062–3067 (2017).
17. M. R. Warke *et al.*, The great oxidation event preceded a Paleoproterozoic "snowball Earth". *Proc. Natl. Acad. Sci. U.S.A.* **117**, 13314–13320 (2020).
18. J. Farquhar, B. A. Wing, Multiple sulfur isotopes and the evolution of the atmosphere. *Earth Planet. Sci. Lett.* **213**, 1–13 (2003).
19. J. Savarino, A. Romero, J. Cole-Dai, S. Bekki, M. H. Thiemens, UV induced mass-independent sulfur isotope fractionation in stratospheric volcanic sulfate. *Geophys. Res. Lett.* **30**, 2131 (2003).
20. E. Gautier, J. Savarino, J. Erbland, J. Farquhar, SO$_2$ oxidation kinetics leave a consistent isotopic imprint on volcanic ice core sulfate. *J. Geophys. Res.* **123**, 9801–9812 (2018).
21. A. Burke *et al.*, Stratospheric eruptions from tropical and extra-tropical volcanoes constrained using high-resolution sulfur isotopes in ice cores. *Earth Planet. Sci. Lett.* **521**, 113–119 (2019).
22. R. Shaheen *et al.*, Large sulfur-isotope anomaly in nonvolcanic sulfate aerosol and its implications for the Archean atmosphere. *Proc. Natl. Acad. Sci. U.S.A.* **111**, 11979–11983 (2014).
23. M. Lin *et al.*, Atmospheric sulfur isotopic anomalies recorded at Mt. Everest across the Anthropocene. *Proc. Natl. Acad. Sci. U.S.A.* **115**, 6964–6969 (2018).
24. T. Hansen, R. B. Farrand, H. A. Montgomery, H. G. Billman, G. Blechschmidt, Sedimentology and extinction patterns across the Cretaceous-Tertiary boundary interval in east Texas. *Cretac. Res.* **8**, 229–252 (1987).

25. T. A. Hansen, B. Upshaw, E. G. Kauffman, W. Gose, Patterns of molluscan extinction and recovery across the Cretaceous-Tertiary Boundary in East Texas: Report on new outcrops. *Cretac. Res.* **14**, 685–706 (1993).

26. M. B. Hart *et al.*, The Cretaceous-Paleogene Boundary on the Brazos River, Texas: New sections and revised interpretations. *Gulf Coast Assoc. Geol. Soc. J.* **1**, 69–80 (2012).

27. J. D. Witts *et al.*, Cephalopods from the Cretaceous-Paleogene (K-Pg) boundary interval on the Brazos River, Texas, and extinction of the ammonites. *Am. Mus. Novit.* **2020**, 1–52 (2021).

28. T. E. Yancey, C. Liu, Impact-induced sediment deposition on an offshore, mud-substrate continental shelf, Cretaceous–Paleogene boundary, Brazos River, Texas, U.S.A. *J. Sediment. Res.* **83**, 354–367 (2013).

29. T. E. Yancey, R. N. Guillemette, Carbonate accretionary lapilli in distal deposits of the Chicxulub impact event. *Geol. Soc. Am. Bull.* **120**, 1105–1118 (2008).

30. P. Schulte, R. Speijer, H. Mai, A. Kontny, The Cretaceous–Paleogene (K–P) boundary at Brazos, Texas: Sequence stratigraphy, depositional events and the Chicxulub impact. *Sediment. Geol.* **184**, 77–109 (2006).

31. A. L. Masterson, B. A. Wing, A. Paytan, J. Farquhar, D. T. Johnston, The minor sulfur isotope composition of Cretaceous and Cenozoic seawater sulfate. *Paleoceanography* **31**, 779–788 (2016).

32. D. A. Kring, M. J. Whitehouse, M. Schmieder, Microbial sulfur isotope fractionation in the chicxulub hydrothermal system. *Astrobiology* **21**, 103–114 (2021).

33. D. Heymann *et al.*, Geochemical markers of the Cretaceous-Tertiary boundary event at Brazos River, Texas, USA. *Geochim. Cosmochim. Acta* **62**, 173–181 (1998).

34. A. L. Zerkle, J. Farquhar, D. T. Johnston, R. P. Cox, D. E. Canfield, Fractionation of multiple sulfur isotopes during phototrophic oxidation of sulfide and elemental sulfur by a green sulfur bacterium. *Geochim. Cosmochim. Acta* **73**, 291–306 (2009).

35. D. T. Johnston, Multiple sulfur isotopes and the evolution of Earth's surface sulfur cycle. *Earth Sci. Rev.* **106**, 161–183 (2011).

36. S. Ono, B. Wing, D. Johnston, J. Farquhar, D. Rumble, Mass-dependent fractionation of quadruple stable sulfur isotope system as a new tracer of sulfur biogeochemical cycles. *Geochim. Cosmochim. Acta* **70**, 2238–2252 (2006).

37. J. Farquhar, D. T. Johnston, B. A. Wing, Implications of conservation of mass effects on mass-dependent isotope fractionations: Influence of network structure on sulfur isotope phase space of dissimilatory sulfate reduction. *Geochim. Cosmochim. Acta* **71**, 5862–5875 (2007).

38. G. Zhang *et al.*, Redox chemistry changes in the Panthalassic Ocean linked to the end-Permian mass extinction and delayed Early Triassic biotic recovery. *Proc. Natl. Acad. Sci. U.S.A.* **114**, 1806–1810 (2017).

39. H. Oduro *et al.*, Evidence of magnetic isotope effects during thermochemical sulfate reduction. *Proc. Natl. Acad. Sci. U.S.A.* **108**, 17635–17638 (2011).

40. M. W. Claire *et al.*, Modeling the signature of sulfur mass-independent fractionation produced in the Archean atmosphere. *Geochim. Cosmochim. Acta* **141**, 365–380 (2014).

41. C. C.-W. Lee, J. Savarino, H. Cachier, M. H. Thiemens, Sulfur (^{32}S, ^{33}S, ^{34}S, ^{36}S) and oxygen (^{16}O, ^{17}O, ^{18}O) isotopic ratios of primary sulfate produced from combustion processes. *Tellus B Chem. Phys. Meterol.* **54**, 193–200 (2002).

42. P. J. Crutzen, The possible importance of CSO for the sulfate layer of the stratosphere. *Geophys. Res. Lett.* **3**, 73–76 (1976).

43. C. Brühl, J. Lelieveld, P. J. Crutzen, H. Tost, The role of carbonyl sulphide as a source of stratospheric sulphate aerosol and its impact on climate. *Atmos. Chem. Phys.* **12**, 1239–1253 (2012).

44. E. Pierazzo *et al.*, Ozone perturbation from medium-size asteroid impacts in the ocean. *Earth Planet. Sci. Lett.* **299**, 263–272 (2010).

45. G. Izon *et al.*, Biological regulation of atmospheric chemistry en route to planetary oxygenation. *Proc. Natl. Acad. Sci. U.S.A.* **114**, E2571–E2579 (2017).

46. I. N. Bindeman, J. M. Eiler, B. A. Wing, J. Farquhar, Rare sulfur and triple oxygen isotope geochemistry of volcanogenic sulfate aerosols. *Geochim. Cosmochim. Acta* **71**, 2326–2343 (2007).

47. I. J. Glasspool, A. C. Scott, Phanerozoic concentrations of atmospheric oxygen reconstructed from sedimentary charcoal. *Nat. Geosci.* **3**, 627–630 (2010).

48. J. D. Witts *et al.*, The impact of the Cretaceous–Paleogene (K-Pg) mass extinction event on the global sulfur cycle: Evidence from Seymour Island, Antarctica. *Geochim. Cosmochim. Acta* **230**, 17–45 (2018).

49. V. Pasquier, R. N. Bryant, D. A. Fike, I. Halevy, Strong local, not global, controls on marine pyrite sulfur isotopes. *Sci. Adv.* **7**, eabb7403 (2021).

50. C. T. Reinhard, N. J. Planavsky, T. W. Lyons, Long-term sedimentary recycling of rare sulphur isotope anomalies. *Nature* **497**, 100–103 (2013).

51. S. Ohno *et al.*, Production of sulphate-rich vapour during the Chicxulub impact and implications for ocean acidification. *Nat. Geosci.* **7**, 279–282 (2014).

52. C. J. Sprain *et al.*, The eruptive tempo of Deccan volcanism in relation to the Cretaceous-Paleogene boundary. *Science* **363**, 866–870 (2019).

53. B. Schoene *et al.*, U-Pb constraints on pulsed eruption of the Deccan Traps across the end-Cretaceous mass extinction. *Science* **363**, 862–866 (2019).

54. P. M. Hull *et al.*, On impact and volcanism across the Cretaceous-Paleogene boundary. *Science* **367**, 266–272 (2020).

55. A. Schmidt *et al.*, Selective environmental stress from sulphur emitted by continental flood basalt eruptions. *Nat. Geosci.* **9**, 77–82 (2015).

56. J. Vellekoop *et al.*, Rapid short-term cooling following the Chicxulub impact at the Cretaceous-Paleogene boundary. *Proc. Natl. Acad. Sci. U.S.A.* **111**, 7537–7541 (2014).

57. D. E. Canfield, R. Raiswell, J. T. Westrich, C. M. Reaves, R. A. Berner, The use of chromium reduction in the analysis of reduced inorganic sulfur in sediments and shales. *Chem. Geol.* **54**, 149–155 (1986).

58. K. A. Baublys, S. D. Golding, E. Young, B. S. Kamber, Simultaneous determination of $\delta^{33}S_{(V-CDT)}$ and $\delta^{34}S_{(V-CDT)}$ using masses 48, 49 and 50 on a continuous flow isotope ratio mass spectrometer. *Rapid Commun. Mass Spectrom.* **18**, 2765–2769 (2004).

59. T. B. Coplen *et al.*, New guidelines for δ^{13}C measurements. *Anal. Chem.* **78**, 2439–2441 (2006).

60. C. Defouilloy, P. Cartigny, N. Assayag, F. Moynier, J.-A. Barrat, High-precision sulfur isotope composition of enstatite meteorites and implications for the formation and evolution of their parent bodies. *Geochim. Cosmochim. Acta* **172**, 393–409 (2015).

61. Y. Ueno, S. Aoyama, Y. Endo, F. Matsu'ura, J. Foriel, Rapid quadruple sulfur isotope analysis at the sub-micromole level by a flash heating with CoF$_3$. *Chem. Geol.* **419**, 29–35 (2015).

62. L. Woelders, R. P. Speijer, Stable seafloor conditions, sea level and food supply during the latest Maastrichtian at Brazos River, Texas. *Mar. Micropaleontol.* **121**, 41–51 (2015).

63. R. V. Demicco, T. K. Lowenstein, L. A. Hardie, R. J. Spencer, Model of seawater composition for the Phanerozoic. *Geology* **33**, 877–880 (2005).

64. M. N. Timofeeff, T. K. Lowenstein, M. A. M. da Silva, N. B. Harris, Secular variation in the major-ion chemistry of seawater: Evidence from fluid inclusions in Cretaceous halites. *Geochim. Cosmochim. Acta* **70**, 1977–1994 (2006).

65. U. G. Wortmann, A. Paytan, Rapid variability of seawater chemistry over the past 130 million years. *Science* **337**, 334–336 (2012).

66. T. J. Algeo, G. M. Luo, H. Y. Song, T. W. Lyons, D. E. Canfield, Reconstruction of secular variation in seawater sulfate concentrations. *Biogeosciences* **12**, 2131–2151 (2015).

67. R. Slingerland *et al.*, Estuarine circulation in the Turonian Western Interior seaway of North America. *Geol. Soc. Am. Bull.* **108**, 941–952 (1996).